NRF2 promotes neuronal survival in neurodegeneration and acute nerve damage

Wenjun Xiong,[1] Alexandra E. MacColl Garfinkel,[1] Yiqing Li,[2] Larry I. Benowitz,[2] and Constance L. Cepko[1]

[1]Departments of Genetics and Ophthalmology, Howard Hughes Medical Institute, Harvard Medical School, Boston, Massachusetts, USA. [2]Boston Children's Hospital, F.M. Kirby Neurobiology Center, Center for Life Science, Departments of Neurosurgery and Ophthalmology, Harvard Medical School, Boston, Massachusetts, USA.

Oxidative stress contributes to the loss of neurons in many disease conditions as well as during normal aging; however, small-molecule agents that reduce oxidation have not been successful in preventing neurodegeneration. Moreover, even if an efficacious systemic reduction of reactive oxygen and/or nitrogen species (ROS/NOS) could be achieved, detrimental side effects are likely, as these molecules regulate normal physiological processes. A more effective and targeted approach might be to augment the endogenous antioxidant defense mechanism only in the cells that suffer from oxidation. Here, we created several adeno-associated virus (AAV) vectors to deliver genes that combat oxidation. These vectors encode the transcription factors NRF2 and/or PGC1a, which regulate hundreds of genes that combat oxidation and other forms of stress, or enzymes such as superoxide dismutase 2 (SOD2) and catalase, which directly detoxify ROS. We tested the effectiveness of this approach in 3 models of photoreceptor degeneration and in a nerve crush model. AAV-mediated delivery of NRF2 was more effective than SOD2 and catalase, while expression of PGC1a accelerated photoreceptor death. Since the NRF2-mediated neuroprotective effects extended to photoreceptors and retinal ganglion cells, which are 2 very different types of neurons, these results suggest that this targeted approach may be broadly applicable to many diseases in which cells suffer from oxidative damage.

Introduction

Oxidative stress has been observed in many degenerative conditions as well as in normal aging. This type of stress leads to damaged proteins, nucleic acids, and lipids, and thus it is not surprising that oxidative stress has been shown to contribute to pathology in multiple instances (1–3). These findings have made oxidative stress an attractive therapeutic target. However, present approaches to reduce oxidative damage, such as providing high doses of exogenous antioxidants, have demonstrated little therapeutic efficacy in clinical trials (4–7). Limited clinical success does not argue against oxidative stress as a contributor to pathogenesis, but rather that a small-molecule approach to reduce oxidation may not be an appropriate one. Few synthetic antioxidants reach a high steady-state systemic level, particularly in the nervous system, where the blood-brain barrier limits access (8). Moreover, even if high levels can be achieved and sustained, reducing reactive oxygen and nitrogen species (ROS/NOS) systemically may be too blunt a strategy, as these molecules have normal physiological roles in signaling, in addition to their pathological effects (9). Local antioxidant therapy utilizing the genes that normally combat oxidative damage has the potential to provide a more specific and effective approach.

Antioxidative proteins can be categorized into 2 groups based on their function. One group comprises the ROS-detoxifying enzymes, including superoxide dismutases (SODs), glutathione peroxidases (GPXs), and catalase. They can clear specific ROS from different cellular compartments and are among the most potent enzymes known. For example, SOD2 converts superoxide radicals (O_2^-), the major form of ROS in living cells, into H_2O_2 and O_2 in mitochondria, while catalase removes H_2O_2 generated during lipid breakdown in peroxisomes. These enzymes are normally expressed in all cells and are subject to transcriptional regulation, which is executed by the other group of antioxidant proteins, transcription factors (TFs) such as peroxisome proliferator–activated receptor γ coactivator 1-α (PGC1a) and nuclear factor erythroid–derived 2, like 2 (NRF2, also known as NFE2L2) (10, 11). PGC1a and NRF2 are 2 master TFs that globally regulate antioxidant defense responses. PGC1a is a multifunctional transcriptional coactivator that also regulates mitochondrial biogenesis and respiration (12). NRF2 boosts the expression of many detoxifying, cytoprotective, and antiinflammatory genes by binding to the antioxidant response element (ARE) in their regulatory regions (13). NRF2 acts via an "on-demand" mechanism that is mediated by cytoplasmic suppression by KEAP1 under physiological conditions, with nuclear accumulation upon stimulation by oxidation (14). Both groups of antioxidant genes have been proposed as therapeutic candidates, e.g., for neurodegenerative disorders, diabetic complications, and cardiovascular diseases, with the hope that the enzymes would be more specific, generating fewer side effects than chemical antioxidants, and that the TFs would provide a broad defense by activating hundreds of genes (15–17). However, only a few studies have been conducted to test this therapeutic strategy by gene delivery via viral vectors in animal models in vivo (18–25), and no studies have compared the effectiveness of the enzymes versus the TFs, or NRF2 versus PGC1a.

▶ Related Commentary: p. 1390

Conflict of interest: The authors have declared that no conflict of interest exists.
Submitted: November 4, 2014; **Accepted:** February 5, 2015.
Reference information: *J Clin Invest*. 2015;125(4):1433–1445. doi:10.1172/JCI79735.

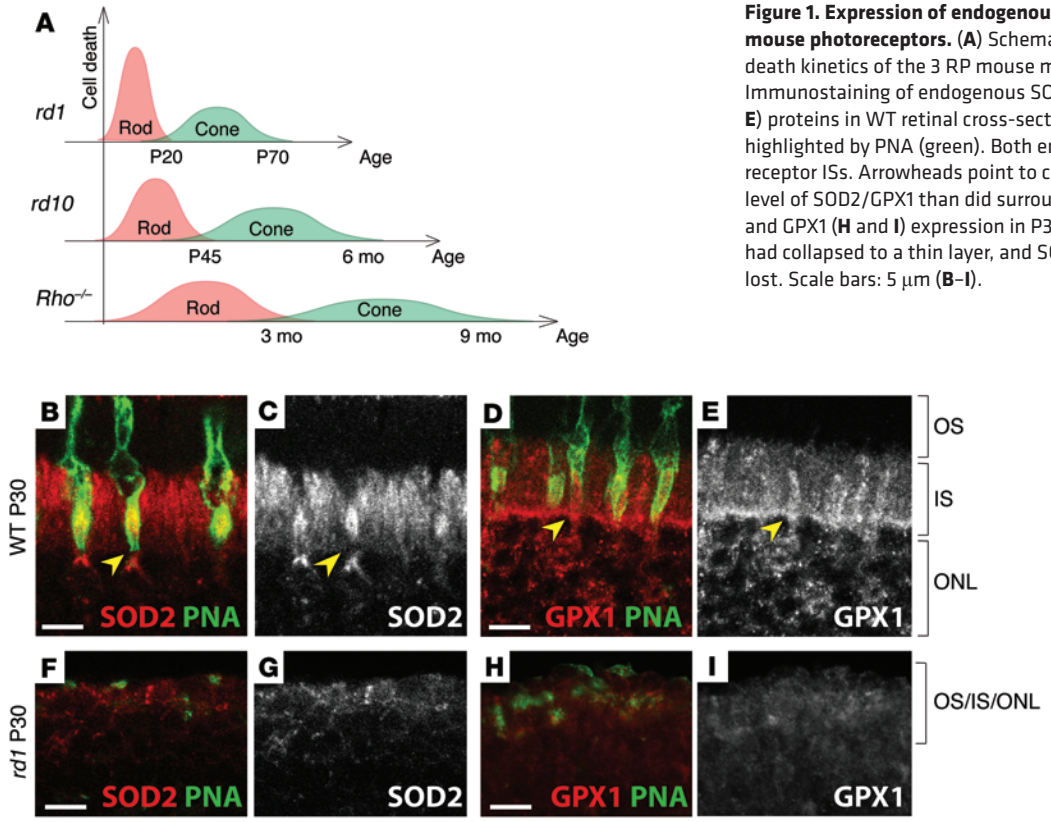

Figure 1. Expression of endogenous antioxidative enzymes in mouse photoreceptors. (**A**) Schematic illustration of rod and cone death kinetics of the 3 RP mouse models used in this study. (**B**–**E**) Immunostaining of endogenous SOD2 (**B** and **C**) and GPX1 (**D** and **E**) proteins in WT retinal cross-sections. Cone OSs and ISs are highlighted by PNA (green). Both enzymes were enriched in photoreceptor ISs. Arrowheads point to cones, which expressed a higher level of SOD2/GPX1 than did surrounding rods. (**F**–**I**) SOD2 (**F** and **G**) and GPX1 (**H** and **I**) expression in P30 *rd1* retina. OSs, ISs, and ONLs had collapsed to a thin layer, and SOD2/GPX1 expression was mostly lost. Scale bars: 5 μm (**B**–**I**).

We developed and compared gene therapies using different antioxidant genes, SOD2/catalase, PGC1a, and NRF2 in murine models of an inherited retinal degeneration disease, retinitis pigmentosa (RP), as well as in a model of nerve crush damage. The key neuronal cell type that undergoes degeneration in most inherited forms of blindness is the cone photoreceptor, which mediates high-acuity and color vision (26). Such inherited diseases are genetically heterogeneous, with at least 60 loci identified in humans for RP, one of the more common forms of inherited blindness (27). Most of the RP genes primarily or exclusively affect the rod photoreceptor, which mediates vision in low light conditions. RP thus first manifests as reduced or absent night vision, as rods are dysfunctional and typically die early during the course of the disease (28). Following rod death, cones lose activity and degenerate, resulting in the progressive loss of daylight vision. Although not all of the mechanisms that lead to the nonautonomous cone death are known, one contributor is oxidative stress. Cones have been shown to have oxidized lipids, nucleic acids, and proteins in RP (29, 30). Oxidative stress has been linked causally to the death of cones in RP, as transgenic overexpression of antioxidant enzymes or repeated injections of antioxidants have been shown to slow down cone degeneration in RP mouse models (30, 31). The fact that there are so many disease genes for RP and that cones are not directly affected by the disease genes, but rather are killed by a nonautonomous effect(s), argues for a generic therapeutic approach to enhance cone survival. An effective antioxidation strategy might provide one such generic approach.

Neurons are also very sensitive to damage to their axons, as occurs in spinal cord injury or in pathologic conditions that increase pressure, e.g., glaucoma (32). Oxidative damage also has been observed in such conditions, and thus antioxidation strategies may prove beneficial for these cases as well (33–35). Whereas photoreceptor cells are highly specialized and unusual neurons, retinal ganglion cells (RGCs) are more typical of the types of CNS projection neurons that suffer damage in acute crush injuries. They have long axons that project to distant targets, as do spinal cord motor neurons. A popular way to model nerve crush damage is to sever the optic nerve, and thus the RGC axons, whereupon the RGCs die within 2 weeks (36–39). This then provides an excellent model of axonal injury.

Using adeno-associated virus (AAV) vectors, we delivered SOD2, catalase, PGC1a, and NRF2, in combination or separately, to cone photoreceptors of 3 different RP mouse models and to RGCs suffering from a nerve crush. We found that antioxidant AAV vectors can slow down cone degeneration and preserve cone morphology in mouse models of RP. Overexpression of NRF2 alone exhibited the most potent rescue effect, while overexpression of PGC1a had an unexpected detrimental effect. Overexpression of SOD2 plus catalase, or overexpression of NRF2 alone, effectively preserved the survival of RGCs following nerve crush. These results demonstrate that AAV-mediated antioxidant gene therapy, particularly with NRF2, may be an effective treatment for multiple cell types across a broad spectrum of diseases that involve oxidation.

Results

Expression of antioxidative enzymes in RP mouse models. In WT retinae, photoreceptors express high levels of antioxidant enzymes, including SOD2 and GPX1, which concentrate in their inner segments (ISs) (Figure 1, B–E). These observations are in keeping with the fact that the ISs of photoreceptors have a notably high density

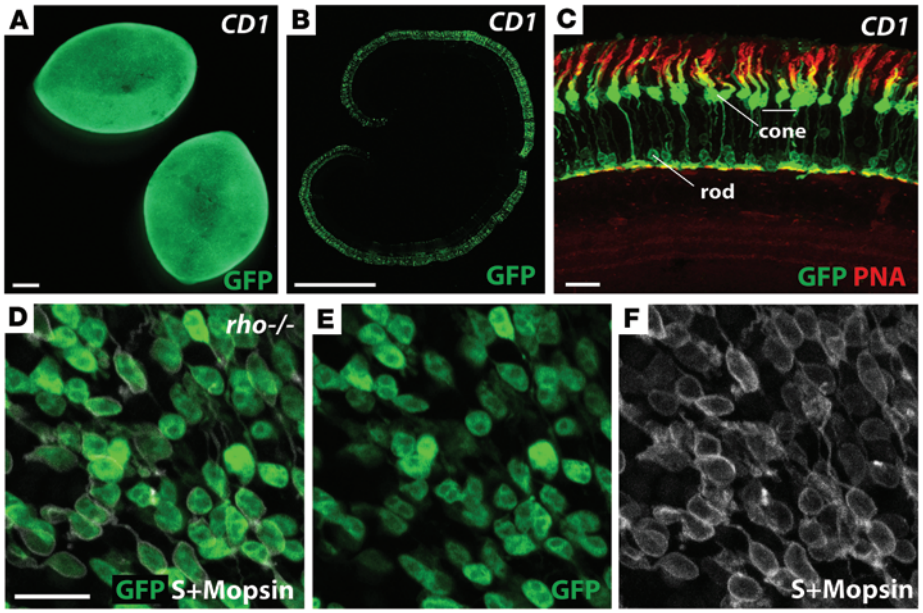

Figure 2. Cones express a high level of GFP from an AAV8 with a CMV promoter. (**A**) Dissected retinae were imaged for GFP fluorescence (green) driven by AAV-GFP, following infection at P0 and imaging at P30. (**B**) Cross-section of an AAV-GFP–infected retina. The ONL shows a high degree of infection (green). (**C**) High-magnification image of a retinal cross-section showing bright GFP in nearly all cones (colabeled with PNA in red) and weak GFP expression in some rods. (**D**–**F**) Short- and medium-wavelength opsin staining (S+M opsin, shown in white) of a 5-month-old *Rho*$^{-/-}$ mouse retina infected with AAV-GFP. Opsin staining coincided with GFP expression in cones. Scale bars: 0.5 mm (**A** and **B**); 20 μm (**C**–**F**).

of mitochondria (40), the major endogenous source of ROS (41). Using shRNA constructs to reduce either of these enzymes in photoreceptors led to an increase in oxidative damage and rapid cell death (Supplemental Figure 1; supplemental material available online with this article; doi:10.1172/JCI79735DS1), demonstrating their importance in photoreceptor survival. Despite the hyperoxic environment and increased oxidative stress experienced by cones during rod degeneration in RP mice (29, 42–44), these antioxidant enzymes were not upregulated (Figure 1, F–I). To provide a specific and long-term approach to enhance the antioxidative capacity of cones, it was possible that AAVs encoding such genes might prolong their survival. We thus selected SOD2 and catalase as an initial set of antioxidant genes, because transgenic overexpression of these 2 enzymes had been reported to promote cone survival in a mouse model of RP (31).

Production of AAV vectors encoding antioxidative enzymes and TFs. In search of a strong promoter for gene expression in cones, we tested GFP reporter expression driven by several types of promoters that are either ubiquitous or specific to photoreceptors (Supplemental Figure 2). AAV vectors (10^{12}–10^{13} genome copies [gc]/ml) were packaged in the serotype 8 capsid, which is effective for photoreceptor infection (45, 46), and were delivered subretinally to P0 mouse eyes. Human CMV immediate-early (IE) promoter, a broadly expressed promoter, drove robust expression in cones. Virtually every cone was brightly labeled by GFP throughout the retina, with some rods and retinal pigment epithelium (RPE) cells also expressing GFP (Figures 2, A–C, and Supplemental Figure 3). GFP expression was observed within 7 days after virus infection and remained high for at least 18 months (Supplemental Figure 4). In fact, GFP expression was so bright and persistent in cones (more so than was opsin protein expression or peanut agglutinin [PNA] staining) that it could be used to track cone survival in diseased retinae at the late stages of degeneration assayed here (Figure 2, D–F). The CMV promoter was thus chosen due to its high activity in cones, as well as for potential additional benefits due to expression in other cell types. To test whether it is possible to mix vectors for combinatorial gene therapy, we further measured the coinfection rate of an AAV-CMV-GFP (referred to hereafter as AAV-GFP) vector and an AAV-tdTomato (referred to hereafter as AAV-tdTomato) vector. The percentage of cones colabeled by GFP and tdTomato was as high as 90% when the titer of each virus was higher than 2×10^{12} gc/ml, which was then set as the concentration for the AAV vectors that were used in the study (Supplemental Figure 5).

Next, we created an AAV vector encoding SOD2 and catalase. Catalase, a peroxisomal protein, was rerouted to mitochondria (31), where it, together with SOD2, can clear superoxide radicals (O_2^-), the main ROS generated during oxidative phosphorylation in the mitochondria. We made and compared 2 sets of vectors. A single AAV vector (AAV-SOD2-2A-Cat) (Figure 3A) that encodes both antioxidant enzymes was made, and an AAV-GFP vector was added at a 1:1 ratio to track infection. In the second set, each gene was encoded by a single AAV vector that also expressed GFP, with GFP expression directed by an IRES element (AAV-SOD2-IRES-GFP and AAV-CAT-IRES-GFP). For both strategies, animals injected with the AAV-GFP vector alone served as the controls. We found that the vectors utilizing an IRES element did not yield high GFP expression, while the combination strategy with separate AAV vectors for each gene produced a high level of expression of GFP and of the antioxidant enzymes, as revealed by IHC on retinal sections (data not shown). We thus used a combination of vectors, with each encoding a single gene for all subsequent experiments. Expression of SOD2 and catalase in GFP$^+$ cells was confirmed by immunostaining for the proteins, and their expression remained robust even at the late stages of degeneration (Figure 3, B–I).

Prolonged cone survival in retinae treated with AAV expressing SOD2 and catalase. We began by evaluating whether overexpression of SOD2 and catalase affected cone survival in *rd1* mice, an RP model with a defective phosphodiesterase β gene that results in early-onset, and rapid, degeneration (47). In *rd1* mice, rods were almost all dead by 3 weeks after birth, and cone death occurred over the next 2 months (Figure 1A). Retinae from AAV-infected mice were harvested at different postnatal days and imaged for native GFP fluorescence. GFP expression in cones showed the stereotypical center-to-periphery progression of cone death in

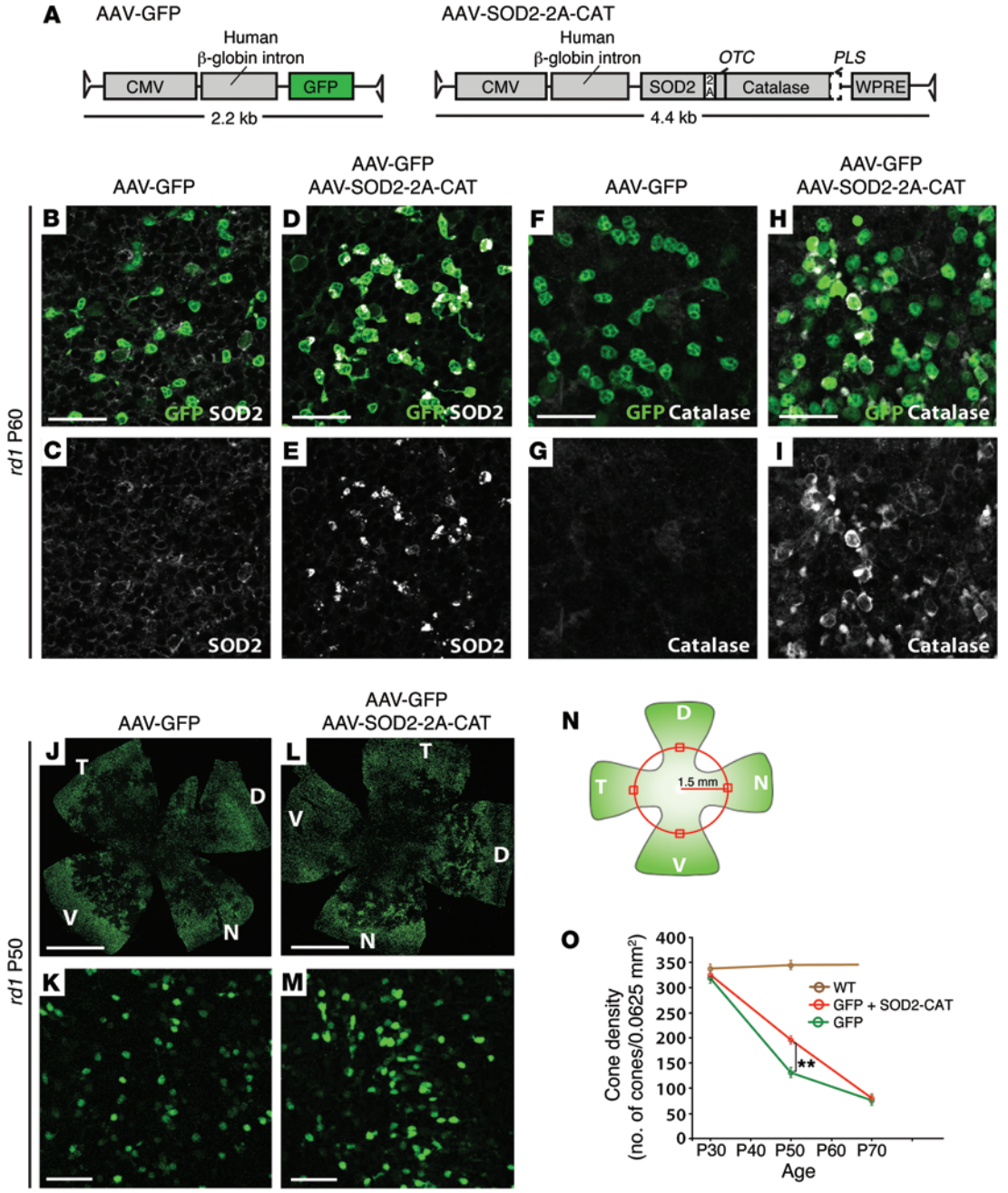

Figure 3. SOD2 and catalase effects on cone survival. (**A**) Schematics of AAV-GFP and AAV-SOD2-2A-CAT constructs. (**B**–**I**) Ectopic SOD2 and catalase expression by AAV vectors was visualized by IHC in flat-mounted P60 *rd1* retinae. (**J** and **L**) Flat-mounted P50 *rd1* retinae infected with AAV vectors expressing GFP (n = 29) (**J**) and GFP, SOD2, and catalase (n = 7) (**L**). D, dorsal; N, nasal; V, ventral; T, temporal. (**K** and **M**) High-magnification images of persisting cones in a 250 μm × 250 μm square from the mid-dorsal retina (1.5 mm dorsal to the optic nerve head) are shown for each group. (**N**) Illustration of the scheme for quantifying cone density. One 250 μm × 250 μm square located 1.5 mm dorsally, nasally, ventrally, and temporally to the optic nerve head was chosen to represent cone survival in each leaflet of the flat-mounted retinae. GFP⁺ cones were counted in each square, and the average number of 4 squares was used for each retina. (**O**) Cone density during the course of *rd1* degeneration. On average, 17 retinae per time point were quantified for each group. Error bars represent the mean ± SEM. $^{**}P < 0.01$ by unpaired 2-tailed Student's t test. Scale bars: 20 μm (**B**–**I**); 1.5 mm (**J** and **L**); 50 μm (**K** and **M**).

this model (ref. 48 and Figure 3, J and L). For evaluation of cone survival, we examined the mid-retinal region (1.5 mm from the optic nerve head), as it represented the average degenerative status of the retina (Figure 3, K and M). To quantify cone density, four 250 μm × 250 μm squares, located 1.5 mm dorsally, nasally, ventrally, and temporally to the optic nerve head, were chosen, as was done previously (31), and the number of bright GFP⁺ cells in the outer portion of each retina was quantified (Figure 3N). Cone densities in both AAV-treated groups were comparable to those of WT (CD1) mice at P30, demonstrating that major cone death had not yet spread to the mid-retina at this stage (Figure 3O). By P50, cone degeneration had rapidly progressed so that, in the

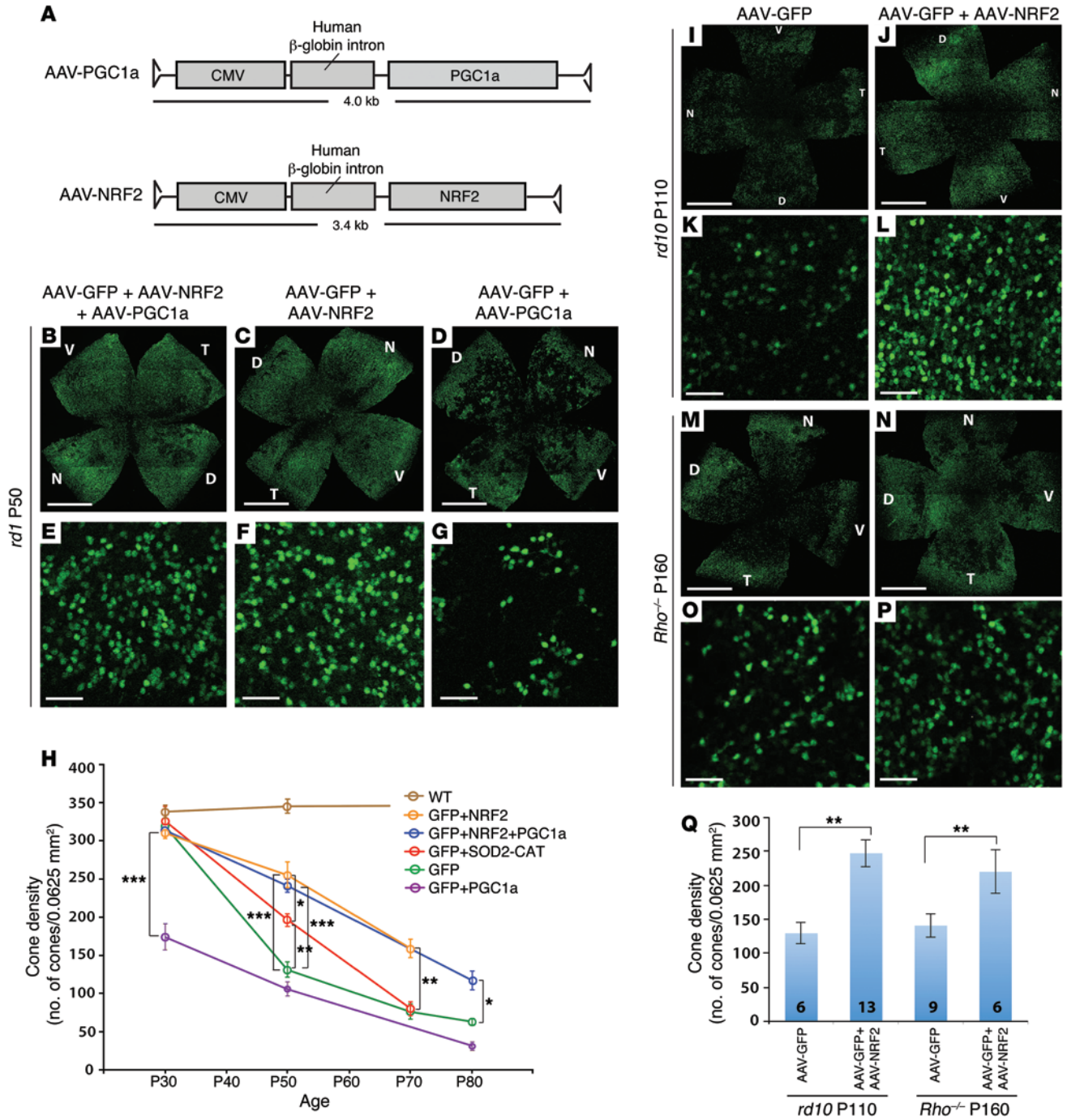

Figure 4. Effects of antioxidative TFs on cone survival. (**A**) Schematics of AAV-PGC1a and AAV-NRF2 constructs. (**B**–**D**) Flat-mounted P50 *rd1* retinae infected with AAV vectors expressing GFP, NRF2, and PGC1a (n = 10) (**B**), GFP and NRF2 (n = 8) (**C**), and GFP and PGC1a (n = 15) (**D**). (**E**–**G**) Persisting cones in the mid-dorsal retina. (**H**) Cone density during the course of *rd1* degeneration following infection with the indicated constructs. Average cone density and number of retinae examined for each group are summarized in Supplemental Table 1. Error bars represent the mean ± SEM. *$P < 0.05$, **$P < 0.01$, and ***$P < 0.0001$ by 2-way ANOVA. (**I** and **J**) Flat-mounted P110 *rd10* retinae infected with AAV vectors expressing GFP (n = 6) (**I**) and GFP and NRF2 (n = 13) (**J**). (**K** and **L**) Higher-magnification images of the mid-dorsal retinae. (**M**–**P**) Flat-mounted P160 *Rho*$^{-/-}$ retinae infected with AAV vectors expressing GFP (n = 9) (**M**) and GFP and NRF2 (n = 6) (**N**), with high-magnification images (**O** and **P**). (**Q**) Quantification of cone density in P110 *rd10* and in P160 *Rho*$^{-/-}$ retinae. The number of retinae quantified for each group is shown at the bottom of each bar. Error bars represent the mean ± SEM. **$P < 0.01$ by unpaired 2-tailed Student's t test. Scale bars: 1.5 mm (**B**–**D**, **I**, **J**, **M**, and **N**); 50 μm (**E**–**G**, **K**, **L**, **O**, and **P**).

mid-retina, the cone numbers were markedly reduced in the control *rd1* mice that received only the AAV-GFP vector (Figure 3O). In contrast, AAV-SOD2-2A-CAT–treated retinae had significantly higher cone density than did the GFP controls at P50 (196 ± 8 vs. 131 ± 10 cells/0.0625 mm^2, $P < 0.01$) (Figure 3O). To ensure that the rescue effect was not specific to the mid-dorsal retina, we also quantified cone density in the entire central retina. Although cone degeneration was more advanced in the central region, we none-

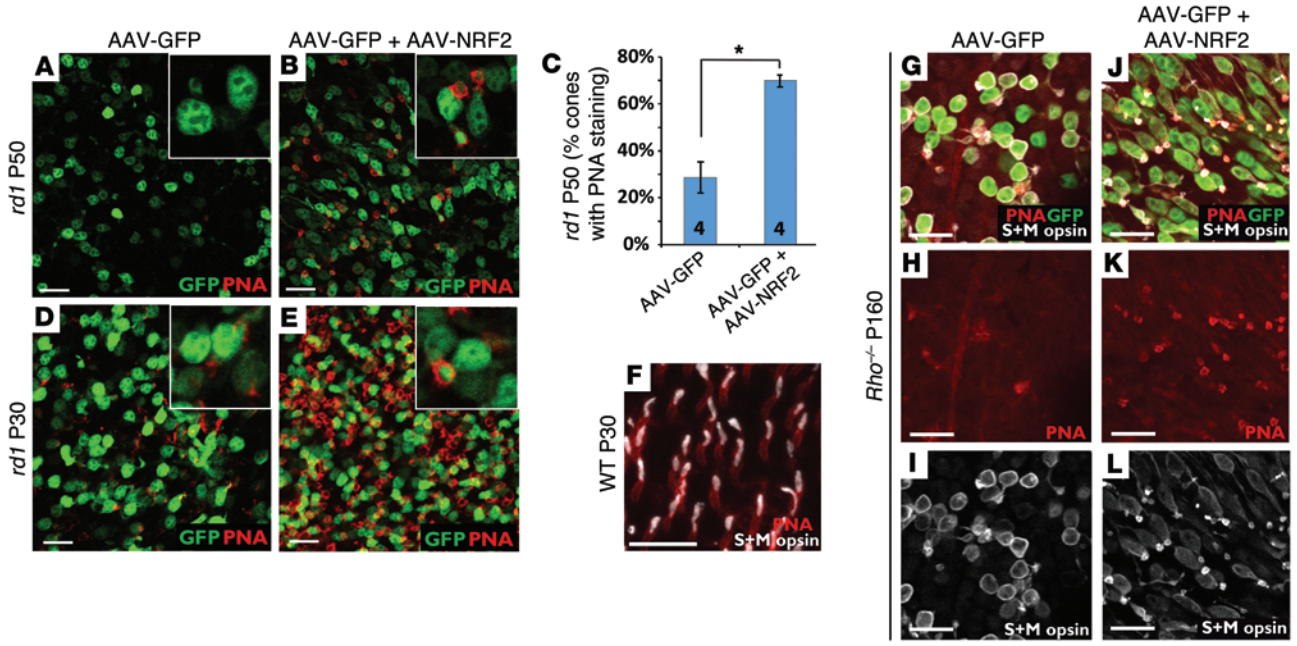

Figure 5. Effect of NRF2 on cone morphology. (**A** and **B**) PNA staining of surviving cones (red) in P50 *rd1* retinae. All images were taken from the mid-dorsal retinal region (~1.5 mm dorsal from the optic nerve head). Insets are high-magnification images of individual cells (original magnification, ×40 for **A**, **B**, **D**, and **E** insets). (**C**) Quantification of the percentages of GFP$^+$ cones with PNA staining in the mid-dorsal region of P50 *rd1* retinae. Approximately 300 cells per retina were counted for each group. Error bars represent the mean ± SEM. The number of retinae quantified is shown in each bar. *$P < 0.05$ by unpaired 2-tailed Student's *t* test. (**D** and **E**) PNA staining of P30 *rd1* retinae. (**F**) PNA (red) and S+M opsin (white) staining in a WT retina. Opsin proteins localized to cone OSs. (**G**–**L**) PNA and opsin staining in P160 *Rho*$^{-/-}$ retinae. Lack of PNA staining and mislocalization of opsins to cell soma were observed in AAV-GFP–infected retinae ($n = 9$) (**G**–**I**), while PNA and opsin colocalized to the remaining cone membrane structures in the retinae infected with AAV-GFP plus AAV-NRF2 ($n = 6$) (**J**–**L**). Scale bars: 20 μm.

theless observed rescue effects similar to those measured in the mid-periphery (Supplemental Figure 6). At P70, a very late stage of *rd1* degeneration, the difference between the SOD2 plus catalase–treated retinae and the control retinae was minimal (80 ± 9 vs. 76 ± 10 cells/0.0625 mm^2, $P > 0.05$) (Figure 3O). These results demonstrate that SOD2 and catalase overexpression can slow down, but not stop, cone death.

Greater cone survival in retinae treated with AAV expressing NRF2 but not PGC1a. Delay of cone death by overexpression of the antioxidant enzymes encouraged us to develop a more efficient antioxidant therapy. Compared with antioxidant enzymes, which work on specific ROS and are restricted to particular cellular compartments, master antioxidant TFs may provide broader, and thus more effective, protection. NRF2 and PGC1a are 2 such TFs, with some overlapping, but largely separate, target genes (10, 13, 14, 49). We made 2 separate AAV vectors (AAV-NRF2 and AAV-PGC1a, Figure 4A) and added them together, or separately, to *rd1* eyes to determine whether they could rescue cone survival. The 2 were tested together to determine whether they worked additively, or even synergistically. We observed cone rescue by NRF2 plus PGC1a, and by NRF2 alone, but not by PGC1a alone (Figure 4, B–G). Overexpression of NRF2 alone resulted in a slightly better rescue than did the 2 genes together, while PGC1a overexpression accelerated cone death, as best seen at the P30 time point (Figure 4H). These results suggest that NRF2 was responsible for the rescue effect seen when the 2 TFs were added together, and thus AAV-NRF2 alone was used for subsequent experiments. Quantification of cone density showed that there were more cones left in the NRF2-treated retinae than in the control retinae (255 ± 17 vs. 131 ± 10 cells/0.0625 mm^2, $P < 0.0001$) or in the SOD2-CAT–treated retinae (255 ± 17 vs. 196 ± 8 cells/0.0625 mm^2, $P < 0.05$) (Figure 4H). The rescue effect seen with NRF2 was also more persistent. At P70, there were still significantly higher cone numbers in the NRF2-treated retinae than in the controls (159 ± 12 vs. 76 ± 10 cells/0.0625 mm^2, $P < 0.001$) (Figure 4H).

To test whether antioxidant therapy could be used to treat RP retinae caused by various genetic lesions, we examined the effect of AAV-NRF2 treatment on cone survival in 2 other RP models: *rd10* and *Rho*$^{-/-}$. *rd10* has a different mutation in the phosphodiesterase β gene and has a slower rate of degeneration than does *rd1* (50). The *Rho*$^{-/-}$ mice are null for the rhodopsin gene, the most common disease-causing gene in autosomal forms of RP (51), and provide a slower model of degeneration than either of the phosphodiesterase β strains. We found that NRF2 overexpression prolonged cone survival in both models (Figure 4, I–Q). This result suggests that antioxidant AAV vectors may be used as a generic therapy for multiple types of RP patients, regardless of their genetic lesion.

Improved morphology in retinae treated with AAV-NRF2. Photoreceptors have specialized morphological domains for the capture of light and phototransduction. The light-sensitive outer segments (OSs) are enriched in phototransduction proteins, while the ISs are densely packed with ribosomes and mitochondria. In diseased retinae, vision is compromised when cone OSs and ISs degenerate, which occurs before cone death. We thus evaluated whether

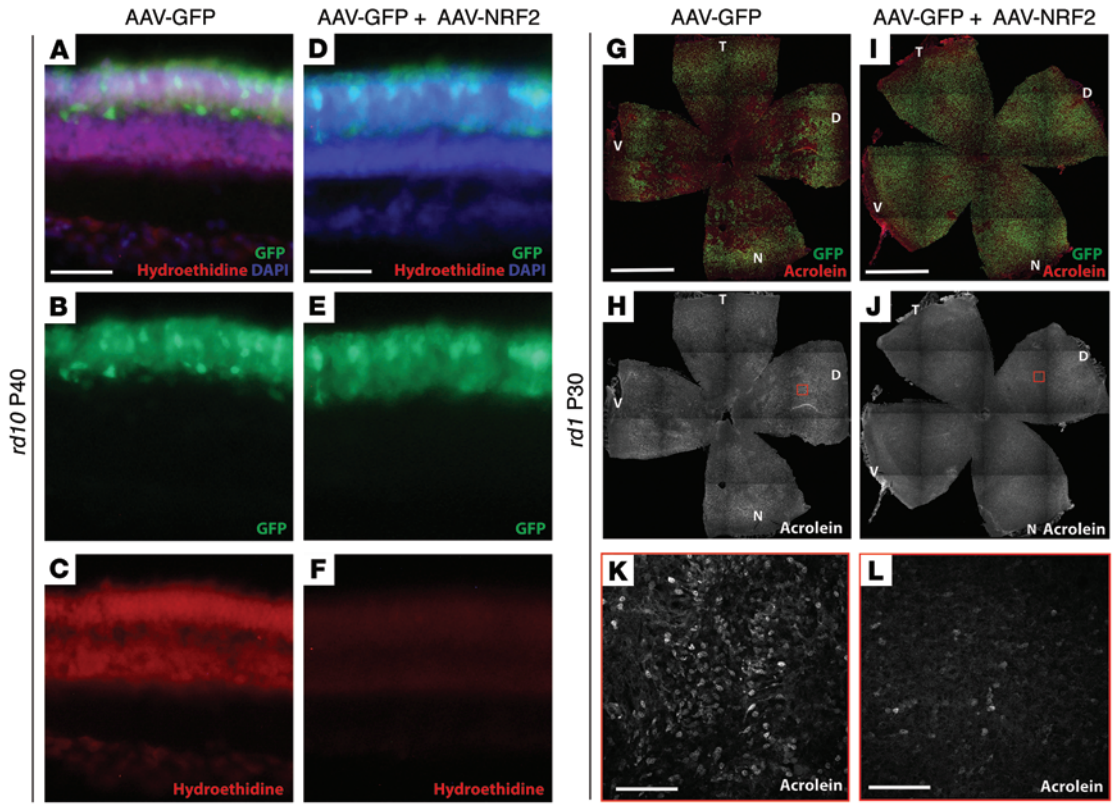

Figure 6. Evaluation of oxidation in AAV-NRF2–treated retinae. (**A**–**F**) Hydroethidine emitted red fluorescence after reacting with superoxide species in the peripheral cross-sections of P40 *rd10* retinae infected with AAV-GFP (**A**–**C**) and AAV-GFP plus AAV-NRF2 (**D**–**F**). (**G**–**L**) Anti-acrolein staining of P30 *rd1* retinae infected with AAV-GFP (**G**, **H**, and **K**) and with AAV-GFP plus AAV-NRF2 (**I**, **J**, and **L**). (**K** and **L**) High-magnification images of the mid-dorsal region in the retinae (highlighted by red frames) shown in **H** and **J**. Scale bars: 20 μm (**A**–**F**, **K**, and **L**); 1.5 mm (**G**–**J**).

antioxidant therapy not only prolongs cone survival, but preserves the structure of cone OSs and ISs as well. The treated retinae were stained with PNA, which outlines cone OSs and ISs. A high percentage of cones in the NRF2-treated *rd1* retinae had PNA-stained structures resembling OSs and ISs, while cones in the control *rd1* retinae lacked PNA^+ structures at P50 (Figure 5, A–C). This observation was made as early as P30 (Figure 5, D and E), before the onset of cone death in *rd1* retinae. We also looked at the opsin proteins, which localized to cone OSs in WT retinae (Figure 5F). However, opsin proteins were shown to mislocalize to cell soma, rather than to OSs, in degenerating retinae (52), as was evident in P160 $Rho^{-/-}$ retinae (Figure 5, G–I). In AAV-NRF2–treated $Rho^{-/-}$ retinae, opsins colocalized with PNA in the OSs and ISs, even though the remaining OS/IS structures were not as long as those in the WT retinae (Figure 5, F–L). Similar results were seen in *rd10* retinae with NRF2 overexpression (data not shown). These observations suggest that antioxidant AAV vectors not only prolong cone survival, but also preserve an important functional domain of cone photoreceptors.

Oxidation is reduced in retinae treated with AAV-NRF2. We next asked whether the rescue effect by antioxidant therapy was associated with reduced oxidation. Using hydroethidine, a dye that emits red fluorescence upon reacting with superoxide radicals, superoxide levels were evaluated in the NRF2-treated and control retinae. There was strong red fluorescence in the control P40 *rd10* retinae, as seen in cross-sections, especially in the outer nuclear layer (ONL) (Figure 6, A–C). In contrast, we found minimal signal in the retina treated with AAV-NRF2 (Figure 6, D–F), suggesting that there was a reduced level of superoxide radicals. Photoreceptor cells are susceptible to oxidative stress, as they have high levels of polyunsaturated fatty acids. We examined the level of lipid peroxidation by immunostaining for acrolein, a marker of lipid peroxidation. The level of acrolein staining was greatly reduced in retinae with NRF2 overexpression (Figure 6, G–L). These results suggest that AAV-NRF2 can effectively protect cones from oxidative damage.

Improved function in retinae treated with AAV-NRF2. To test whether the prolonged survival and preserved morphology effected by antioxidant gene therapy translated into improved vision, we evaluated the visual acuity of *rd10* mice using an optomotor assay (53). The assay was performed under the brightest luminance setting (60 cd/m^2) to assay cone response. We first carried out a time-course study of visual acuity of untreated *rd10* mice and found that their visual acuity dropped quickly between P30 and P60 (Figure 7A, white boxes). The left and right eyes of untreated *rd10* mice consistently showed very similar visual acuity levels (right eye/left eye [R/L] ratio of ≈1), despite the variation among animals (Figure 7B, white bars). Therefore, the uninjected left eyes were used as within-animal controls for the AAV-injected right eyes of the treated mice. We next measured the visual acuity of *rd10* mice treated with AAV-GFP alone or with AAV-GFP plus AAV-NRF2 over the course of degeneration. In all animal groups, we observed a similar rate of decrease in visual acuity in the left eye, while visual acuity in the right eye treated with AAV-GFP plus

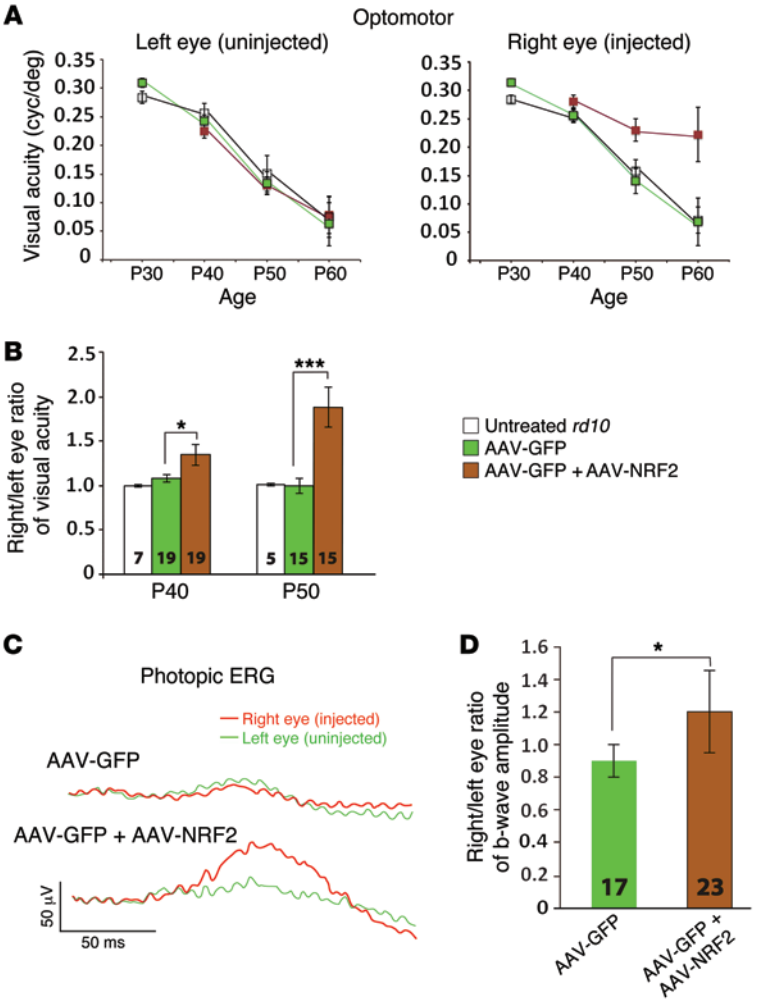

Figure 7. Evaluation of function following infection with AAV-NRF2. (**A**) The optomotor assay was used to test the visual acuity in *rd10* mice that were uninjected or injected with AAV-GFP alone or AAV-GFP plus AAV-NRF2. The left and right eyes are shown separately. (**B**) Ratio of R/L eye visual acuity in *rd10* mice at P40 and P50. (**C** and **D**) Photopic ERG was performed in *rd10* mice at P40. Representative waveforms (**C**) and average R/L eye ratios of b-wave amplitude (**D**) for control (n = 17) and AAV-NRF2–treated (n = 23) mice are shown. The number of mice tested in each group is shown in each bar. Error bars represent the mean ± SEM. $^*P < 0.05$ and $^{***}P < 0.0001$ by unpaired 2-tailed Student's t test.

AAV-NRF2 decreased more slowly (Figure 7A). Our evaluation of the therapeutic effect was based on the ratio of R/L eye visual acuity, which minimized the variations among littermates as well as between litters. An increase in R/L eye visual acuity ratios in the NRF2-treated (1.34 ± 0.12) animals compared with the ratios in the GFP-treated *rd10* animals (1.07 ± 0.04) was observed at P40 (Figure 7B). The difference between treated and untreated eyes became more significant at P50, such that the visual acuity in the right eye of NRF2-treated animals was almost 2 times better than that in the left eye (1.92 ± 0.17 vs. 1.00 ± 0.11) (Figure 7B).

Antioxidant treatment with AAV-NRF2 also led to the preservation of cone function, as shown by the b-wave amplitude when photopic electroretinography (ERG) was performed. Better waveforms and a significantly higher R/L eye ratio of b-wave amplitude were seen at P40 in the NRF2-treated *rd10* retinae than in the GFP control retinae (1.20 ± 0.25 vs. 0.84 ± 0.09, $P < 0.05$) (Figure 7, C and D).

Additional types of neurons can be preserved by AAV-NRF2 gene therapy. Finally, we wanted to determine whether antioxidant gene therapy might be extended to other cell types in which oxidative stress has been implicated in cell death. For example, when nerves are severed or crushed in traumatic accidents, neurons often exhibit oxidative damage (33, 35). We tested the antioxidant AAV vectors in an axonal injury model for RGCs, in which more than 80% of the RGCs die within 2 weeks after optic nerve crush (ONC) (36, 38, 54). In this experiment, GFP, SOD2 plus catalase, or NRF2 AAV vectors were packaged by AAV serotype 2 capsids and delivered intravitreally for RGC expression 14 days before ONC (39). Retinae that received AAV vectors encoding SOD2 and catalase, or those encoding NRF2, retained significantly more RGCs than did the control retinae expressing GFP 2 weeks after ONC (Figure 8, A–C). The rescue effect on RGC survival extended to at least 4 weeks after ONC (Figure 8D). The effect was limited to survival, as axonal regeneration was not promoted by either type of antioxidant vector (Supplemental Figure 7).

Discussion

We have successfully developed an antioxidant gene therapy that prolongs neuronal survival in mouse models of acute and slow neurodegeneration. Overexpression of NRF2, a master antioxidant TF, and overexpression of SOD2 and catalase, 2 antioxidant enzymes, slowed down cone cell death across 3 photoreceptor degeneration models. Importantly, cone morphology and visual function were preserved as well. This rescue effect also was observed in a nerve crush model in which neurons die rapidly due to acute injury to their axons. Since fundamentally different cell types were rescued with these treatments, gene therapy using endogenous antioxidant defense mechanisms may be effective for many types of neurodegenerative diseases. Moreover, these vectors may be beneficial in other tissue and disease types, since NRF2, SOD2 and, catalase are broadly expressed (55).

An important foundation for this study was the work by the Campochiaro group, who demonstrated that daily administration of antioxidants, or transgenic overexpression of SOD2 and catalase, was able to slow cone death in RP mice, e.g., out to P35 in *rd1* mice and to P50 in *rd10* mice (30, 31, 56). Directed and stable expression of antioxidant enzymes or TFs by AAV vectors, which have proven to be safe and effective for ocular gene therapy in clinical trials (57–59), should provide long-term protection for chronic diseases such as RP. As mentioned above, long-term and high doses of antioxidants may have side effects in humans and, in any case, are difficult to achieve and have not been effective in clinical trials (4–7).

Another instructive aspect of this study is the comparison of the rescue effects of 2 master antioxidant TFs, PGC1a and NRF2, with each other, and with SOD2 and catalase. Both of these TFs have been proposed to be survival-promoting agents for neurodegenerative diseases (16, 60). However, there have been no studies comparing their effects and only a few studies that have examined

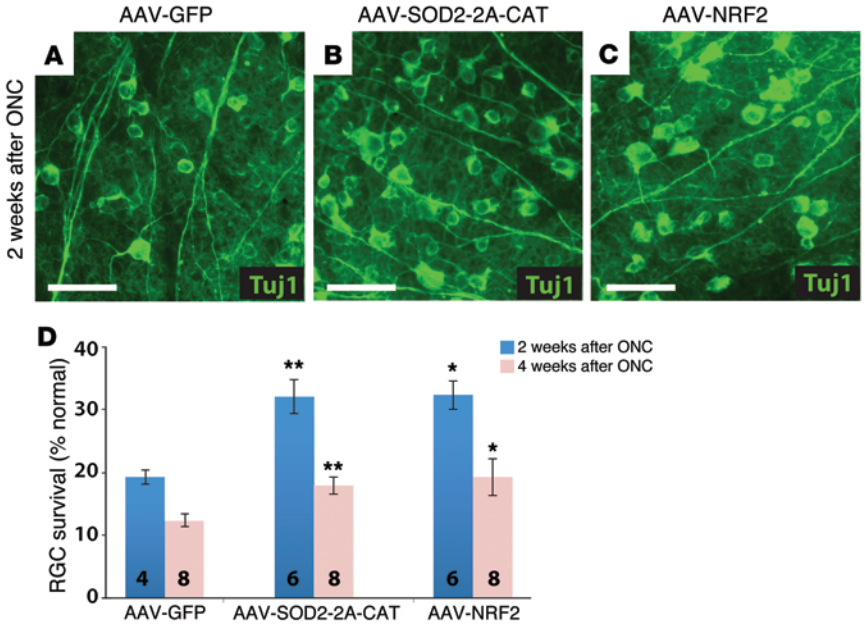

Figure 8. RGC survival at 2 and 4 weeks after ONC. (**A**–**C**) Immunostaining of RGC cells in retinal flat mounts. Two weeks before ONC, the eyes of adult C57Bl/6J mice received an intravitreal injection of AAV2 vectors expressing GFP (n = 4) (**A**), SOD2-2A-CAT (n = 6) (**B**), or NRF2 (n = 6) (**C**). Retinae were harvested 2 weeks after ONC and stained for β3-tubulin (Tuj1) (green), a specific RGC marker. (**D**) Quantification of RGC survival at 2 weeks and 4 weeks after ONC. Numbers were normalized to the WT C57Bl/6J retinae without ONC. The number of retinae examined in each group is shown in each bar. Error bars represent the mean ± SEM. *P < 0.05 and **P < 0.01 by 2-way ANOVA.

the effects of overexpression of either of these genes (18–20, 24, 25). Overexpression of NRF2 alone exhibited a better rescue effect on photoreceptor survival and function than did overexpression of SOD2 and catalase. This result is likely because NRF2 not only promotes the expression of SOD2 and catalase, but also orchestrates the induction of other antioxidant genes, including *Gpx*, peroxiredoxins (*Prx*), and many glutathione- and NADPH-regenerating enzymes, resulting in a broader and more balanced regulation of various ROS intermediates in different cellular compartments (11, 61–63). Beyond antioxidation, NRF2 is also suggested to mediate cytoprotective and antiinflammatory effects via its downstream targets such as NAD(P)H dehydrogenase, quinone 1 (NQO1) and heme oxygenase-1 (HO-1) (11, 61, 62). Our results suggest that small-molecule NRF2 activators, including the FDA-approved drug dimethyl fumarate (BG-12), currently used for multiple sclerosis (64, 65), may be a useful therapeutic agent for retinal degeneration. While it is highly speculative at this point, our results provide the rationale for testing the effects of BG-12 on animal models of RP. In contrast to NRF2 overexpression, PGC1a overexpression accelerated cone death. This result might be due to activities of PGC1a beyond antioxidant regulation, such as induction of angiogenesis (66). However, the reason for the detrimental effect of PGC1a overexpression needs further investigation. Nonetheless, our results are consistent with a report that overexpression of PGC1a led to overt degeneration of dopaminergic neurons in the adult rat nigrostriatal system (67), suggesting that it may be important to keep PGC1a at a physiological level in some cellular contexts. It is also interesting to note that the expression of PGC1a was already high in normal and diseased retinae, whereas NRF2 was undetectable by IHC (data not shown). Thus, the overexpression of PGC1a may send the level over a threshold that cells cannot tolerate.

There is exceptional genetic heterogeneity associated with retinal degeneration diseases, with approximately 200 disease genes and thousands of mutations identified in humans leading to blindness (27). Addressing each genetic deficit would be a difficult and expensive undertaking. Generic gene therapy, such as the antioxidant gene therapy reported here, can be a cost-effective treatment for individuals with RP caused by different genetic lesions and perhaps for individuals with other retinal diseases in which oxidation is present, such as glaucoma and age-related macular generation (AMD) (68, 69). Interestingly, SOD2 knockdown in the RPE induces early AMD phenotypes (70), and many additional lines of evidence suggest that oxidation plays a role in AMD. These vectors may thus be useful in this disease, particularly for dry AMD, which has no effective treatment and is quite common in individuals over the age of 75 (71).

The antioxidant gene therapy demonstrated here can significantly slow down cone death such that, in the fastest model of degeneration, the *rd1* mouse, there are more cones present in the NRF2-treated retinae than in the GFP-treated retinae at P70. It is not clear, however, how to extrapolate these effects to humans. It could be the case that, given the larger retina and slower disease kinetics in humans, cone survival will occur over a much longer period following NRF2 overexpression. However, the antioxidant gene therapies did not completely stop cone degeneration. Cone death in RP is unlikely to be caused only by oxidative stress. Rather, cone death is likely due to a combination of stress factors including, but not limited to, metabolic dysregulation (48), lack of trophic factors (72–76), and inflammation (77). While antioxidant gene therapy can be used as a standalone treatment, it can also supplement other gene therapies. It might be particularly useful in the case of optogenetic therapy (78). Dysfunctional cones in RP mouse models were shown to respond to light that activated an optogenetic protein, halorhodopsin, which was delivered by an AAV (79). Optogenetic therapy is thought not to extend the lifespan of RP cones, but rather to extend the period during which they are functional. Augmenting optogenetic therapy with a survival-promoting therapy, such as that developed here, might extend the period of survival and function. Fortunately, AAV is a suitable vector for such combinatorial gene therapy, as confirmed by our

demonstration of a high coinfection rate (Supplemental Figure 5). In addition to augmenting optogenetic therapy, gene therapy that works against oxidative stress or provides growth factors may also be used as a supplement for stem cell therapy to allow engrafted photoreceptor cells to survive in a noxious host environment.

Many RP patients are not diagnosed until their cones begin to degenerate, when daylight vision is compromised following the loss of many or most rods. In such cases, early intervention, such as gene replacement therapy to save rods, is not possible. In this study, we performed neonatal AAV injection, which has the benefit of allowing the viral inoculum to spread throughout the retina. Future work is needed to determine whether the benefits can be achieved by delaying antioxidant AAV injection, for example, to a time point at which most rods are gone. One promising possibility is that, given the large size of the human eye and the progression of loss of cone vision from the periphery to the center, inoculation into the areas at the advancing front of cone loss will suffice to delay cone degeneration and protect the patient's most valuable central vision. It also will be interesting to examine whether NRF2 overexpression not only rescues cones, but also promotes cone OS regeneration, as cone OSs are the site of phototransduction, and their presence is correlated with function (79).

We also observed a neuroprotective effect of the antioxidant AAV vectors on RGC survival after ONC, a model of acute axonal injury. Acute axonal injury also occurs in spinal cord injury, in which motor neurons are the cell type that is compromised, as they are in several slower, but devastating diseases, such as amyotrophic lateral sclerosis (ALS). Overexpression of NRF2 in stem cell models of ALS showed a benefit, though in vivo delivery was too inefficient to allow an interpretation of effectiveness in vivo (25). Similarly, studies using a lentivirus encoding NRF2 in a mouse model of acute spinal cord injury were inconclusive due to deleterious effects of the lentivirus itself (19). Nonetheless, the occurrence of oxidative damage in these conditions warrants further investigation of the effectiveness of NRF2 overexpression. In the eye, axonal damage in the vicinity of the lamina cribrosa compromises RGCs, leading to their loss and the concomitant loss of vision, as occurs in glaucoma (32). Oxidative stress has been suggested to play a role in the pathogenesis of glaucoma (68). In the ONC model, the presence of superoxide anion is an early sign of RGC apoptosis, and intravitreal injection of polyethylene glycol–conjugated SOD promoted RGC survival up to 2 weeks after axotomy (33). A study of *Nrf2*-deficient mice showed that there was a lower number of RGCs after ONC, supporting the role of NRF2 in protecting RGCs after injury (80). Consistent with these previous studies, the experiments reported here showed that AAV-mediated antioxidant gene therapy prolonged RGC survival.

Oxidative stress is often observed in neurodegenerative disorders, such as Parkinson's Disease (1, 81–83). It likely has an impact on multiple pathological pathways, such as mitochondrial dysfunction and inflammation, and is an important link in the cascade of vicious events that lead to neuronal death. For example, mitochondrial dysfunction caused by complex I deficiency in Parkinson's disease can lead to enhanced production of ROS, which in turn can cause the accumulation of mitochondrial protein damage and mitochondrial DNA mutations that further impair the assembly or function of the respiratory chain (84–86). There is evidence that the NRF2 pathway is among those that are mostly differentially regulated during the course of Parkinson's disease (87, 88), and activation of the NRF2 pathway by small molecules or by transgenic overexpression has been shown to slow down neuronal loss and disease progression in animal models of Parkinson's disease (89, 90). However, there are also alarming reports of NRF2 activation in cancer cells, suggesting a potential risk of systemic upregulation of NRF2 (91, 92). Here, we demonstrate an alternative therapeutic strategy using targeted overexpression of NRF2 via AAV, thereby providing specificity as well as longevity of treatment that may benefit a range of pathological conditions.

Methods

Animals. *CD1* and *rd1* (FVB/N) mice were purchased from Charles River Laboratories. C57Bl/6J and *rd10* mice were purchased from The Jackson Laboratory. *Rho*$^{-/-}$ mice were provided by Janis Lem (Tufts University, Boston, Massachusetts, USA) (51). All mice were kept on a 12-hour light/12-hour dark cycle.

AAV vector construction and virus production. Mouse full-length cDNA clones of SOD2 (MMM4769-99609684) and catalase (MMM-4769-99609855) were ordered from Thermo Scientific. The peroxisome targeting signal (PTS) (aa sequence GSHMAAKGKANL) of catalase was removed, and the mitochondrial targeting sequence (referred to as OTC; forward primer: 5′-AAGAATTCATGCTGTTTA-ATCTGAGGATCCTGTTAAACAATGCAGCTTTTAGAAATGGTC ACAACTTCATGGTTCGAAATTTTCGGTGTGGACAACCACTAC AATCGGACAGTCGGGACCCAGC-3′; reverse primer: 5′-ATATGC-GGCCGCTTAGGCCTGCGTGTAGGTGTGA-3′) from the ornithine transcarbamoylase gene was added following a PCR reaction, as previously described (31). SOD2, 2A (the self-cleaving peptide for gene coexpression; ref. 93), and catalase sequences were ligated together using Gibson Assembly Master Mix (New England BioLabs), and the entire SOD2-2A-CAT sequence was cloned into AAV-MCS8 empty vector (Harvard Medical School DF/HCC DNA Resource Core) via EcoRI/NotI sites. Woodchuck hepatitis virus posttranscriptional element (WPRE) was inserted at the 3′ end of the cassette for enhanced expression. The mouse cDNA clone of NRF2 (MMM1013-202763164) was obtained from Thermo Scientific and inserted into the AAV-MCS8 vector with NotI restriction sites added to both the 5′ and 3′ ends. Mouse *Ppargc1a* cDNA was provided by Bruce Spiegelman (Dana Farber Cancer Institute, Boston, Massachusetts, USA) and was cloned into AAV-MCS8 via NotI/XhoI sites. AAV-CMV-GFP vector plasmid was obtained from the Harvard DF/HCC DNA Resource Core (clone ID: EvNO00061595) and contained a human CMV enhancer/promoter, human β-globin intron, and GFP cDNA.

Recombinant AAV8 and AAV2 vectors were produced as previously described (94). Briefly, AAV vector, rep/cap packaging plasmid, and adenoviral helper plasmid were mixed with polyethylenimine and added to HEK293T cells (catalog HCL4517; Thermo Scientific). Seventy-two hours after transfection, supernatant was collected for AAV8 preparations, and cells were harvested for AAV2 preparations (95). AAV8 viruses in the supernatant were precipitated (mixed with 8.5% w/v PEG-6000 and 0.4 M NaCl for 2 hours at 4°C), centrifuged at 7,000 *g* for 10 minutes, and resuspended in virus buffer (150 mM NaCl and 20 mM Tris, pH 8.0). For AAV2 viruses, the cell pellet was resuspended in virus buffer, followed by 3 cycles of freeze-thawing, and Dounce homogenized. Cell debris was pelleted at 5,000 *g* for 20 minutes, and the supernatant

was run on an iodixanol gradient. Recovered AAV vectors were washed 3 times with PBS using Amicon 100K columns (EMD Millipore). RT-PCRs and protein gels were run to determine virus titers. Viruses were diluted to various concentrations to test infection, and a concentration of approximately 2×10^{12} gc/ml was used for the rescue experiments. AAV8-CMV (SV40 intron)–GFP plasmid (plasmid ID: PV0101) used in Supplemental Figure 3 was obtained from the University of Pennsylvania Vector Core (Philadelphia, Pennsylvania, USA), and the AAV8 serotype-packaged viruses were a gift of the Gene Transfer Vector Core (Schepens Eye Institute, Boston, Massachusetts, USA)

AAV injection. Subretinal injection into P0 neonate eyes was performed as previously described (96, 97). Approximately 0.3 μl AAV8 (10^{12}–10^{13} gc/ml) was introduced into the subretinal space using a pulled angled glass pipette controlled by a FemtoJet (Eppendorf). The left eyes were uninjected for within-animal controls.

Optomotor assay. Visual acuity was measured using an Optometry System (CerebralMechanics Inc.) as previously described (53). All tests were performed between 9 am and 2 pm. Mice were placed on the platform and allowed to habituate to the chamber for 5 minutes. They were assessed for reflexive head-tracking movements in concert with the rate of a virtual sine wave grating on the surrounding monitors, and the visual acuity threshold was determined at the highest spatial frequency (cycle/degree) when the animal stopped tracking. Testing was done with a grating of 12 degrees/second drifting speed and 100% contrast. The right and left eyes were tested independently, as they responded separately to counterclockwise and clockwise grating rotations, respectively (98). A staircase procedure was used, in which the observer tested low to high visual acuity. Each animal was tested for 5 to 15 minutes per session, and testing began right after weaning and lasted for 1 to 2 months, until no obvious response was observed in either eye. The individual who tested the animals was blinded to the treatment groups.

ERG. An Espion E3 System (Diagonsys LLC) was used for recording ERGs in *rd10* mice. Mice were anesthetized, and the pupils of both eyes were dilated. Photopic ERG was performed according to a published protocol (31). Mice were light adapted for 10 minutes at a background light of 30 cd/m^2. Cone responses were elicited by a 34 cd × s/m^2 flash light with a low background light of 10 cd/m^2, and signals were averaged from 50 sweeps.

ONC. Adult C57BL/6J mice were obtained from the Jackson Laboratory. Mice received an intravitreal injection of AAV2 vectors at 8 to 10 weeks of age. Intravitreal AAV injection and ONC surgery were performed under general anesthesia as previously described (36). Briefly, approximately 3 μl AAV2-GFP (control vector), AAV2-NRF2, or AAV2-SOD2-2A-CAT (all with ~5×10^{12} gc/ml titer) was injected into both eyes of each mouse. Fourteen days after AAV injection, the optic nerve was crushed for 5 seconds at 0.5 mm from the optic nerve head using forceps. Mice were sacrificed 2 weeks or 4 weeks after the ONC surgery, and their retinae and optic nerves were harvested for IHC to quantify RGC survival and axonal regeneration (see the Supplemental Material for details on the RGC axonal regeneration analysis and quantification method).

Histology. Eyes were enucleated and marked for orientation on the dorsal periphery. Retinae were dissected and fixed in 4% formaldehyde for 30 minutes at room temperature. For retinal sections, fixed retinae were cryoprotected in 5%, 15%, and 30% sucrose in PBS for a few hours and embedded in OCT on dry ice. Sections (20 μm thick) were cut on a cryostat (Leica). Retinal sections or whole retinal cups were blocked in 5% BSA in PBST (PBS with 0.1%Triton X-100), stained with primary antibodies at 4°C overnight, and washed 3 times with PBST. A different blocking solution (TBS with 2% Triton X-100, 1% normal goat serum, and 0.1% SDS) was used for RGC staining. Primary antibodies used in this study included: rabbit anti–cone arrestin (1:250; AB15282; EMD Millipore); rabbit anti-acrolein (1:250; ab37110; Abcam); rabbit anti–red/green opsin (1:300; AB5405; EMD Millipore); goat anti–blue opsin (1:100; sc-14365; Santa Cruz Biotechnology Inc.); rabbit anti-SOD2 (1:250; ab13533; Abcam); rabbit anti-GPX1 (1:250; ab22604; Abcam); rabbit anti-catalase (1:1,000; ABIN96131; antibodies-online); rabbit anti–β3-tublin (1:500; ab18207, Tuj1 clone; Abcam); and rhodamine-conjugated and FITC-conjugated PNA (1:1,000; Vector Laboratories). Sections or whole retinae were stained using secondary antibodies, including donkey anti–rabbit CY3, donkey anti–rabbit Alexa Fluor 647, and donkey anti–goat Alexa Fluor 647 (all used at 1:1,000; Jackson ImmunoResearch), and were costained with DAPI in the dark for 2 hours at room temperature and mounted in Fluoromount-G (SouthernBiotech). Images of flat-mounted retinae were taken using a ×10 objective with tile scans, and all other images were taken using a ×40 objective with *Z*-stacks on a Zeiss LSM780 confocal microscope. Images used for comparison between groups were taken side by side at the same confocal settings.

Statistics. For cone density quantification, retinae were masked for their treatment groups. In each retina, four 250 μm × 250 μm squares, located 1.5 mm dorsally, nasally, ventrally, and temporally to the optic nerve head, were chosen to represent the average cone density in the respective leaflets. The number of bright GFP$^+$ cells was quantified with ImageJ software (NIH). One number, averaged from the 4 squares, represented the cone density for 1 retina. Statistical analysis of cone densities between groups at different stages (Figure 4H) was carried out using 2-way ANOVA. A P value of less than 0.05 was considered statistically significant.

RGC survival was quantified in 8 rectangular areas (420 μm × 560 μm) in the flat-mounted retinae, with 1 image captured 1 mm and 1 captured 2 mm from the optic nerve head in each of the 4 leaflets by a fluorescence microscope (E800; Nikon). Tuj1$^+$ cells were counted using ImageJ software, and cell densities were averaged from 8 areas of 1 eye and normalized to the average number of RGCs in the WT C57BL/6 retinae. Data are represented as mean percentages ± SEM. Statistical analysis between groups was performed using 2-way ANOVA. A P value of less than 0.05 was considered statistically significant.

All other statistical analyses between 2 groups were performed using the unpaired 2-tailed Student's t test. A P value of less than 0.05 was considered statistically significant.

Study approval. All animal procedures performed were approved by the IACUC of Harvard University, and animal care was carried out in accordance with institutional guidelines.

Acknowledgments

We are grateful to Michael Do, Michael Brown, and Greg Bryman for their technical assistance and insightful discussions; Basil Pawlyk and Michael Sandberg for their helpful instructions with the ERG assay; Ru Xiao and Luk Vandenberghe for the discussion on AAV production and infection; and Bruce Spiegelman for the *Ppargc1a* cDNA plasmid and discussion. The AAV8-CMV (SV40 intron)–GFP virus was a gift of the Gene Transfer Vector Core (Schepen Eye Institute, Boston, Massachusetts, USA). This work

was supported by the NIH (RO1 EY023291 and R21 EY024137); the Howard Hughes Medical Institute; and the Dr. Miriam and Sheldon G. Adelson Medical Research Foundation.

Address correspondence to: Constance Cepko, NRB360, 77 Avenue Louis Pasteur, Boston, Massachusetts 02115, USA. Phone: 617.432.7618; E-mail: cepko@genetics.med.harvard.edu.

1. Guzman JN, et al. Oxidant stress evoked by pacemaking in dopaminergic neurons is attenuated by DJ-1. *Nature*. 2010;468(7324):696–700.
2. Nunomura A, et al. Oxidative damage is the earliest event in Alzheimer disease. *J Neuropathol Exp Neurol*. 2001;60(8):759–767.
3. Ferrante RJ, et al. Evidence of increased oxidative damage in both sporadic and familial amyotrophic lateral sclerosis. *J Neurochem*. 1997;69(5):2064–2074.
4. Parkinson Study Group QE3 Investigators, et al. A randomized clinical trial of high-dosage coenzyme Q10 in early Parkinson disease: no evidence of benefit. *JAMA Neurol*. 2014;71(5):543–552.
5. Lloret A, Badía MC, Mora NJ, Pallardó FV, Alonso MD, Viña J. Vitamin E paradox in Alzheimer's disease: it does not prevent loss of cognition and may even be detrimental. *J Alzheimers Dis*. 2009;17(1):143–149.
6. Petersen RC, et al. Vitamin E and Donepezil for the treatment of mild cognitive impairment. *N Engl J Med*. 2005;352(23):2379–2388.
7. Parkinson Study Group. Effects of tocopherol and deprenyl on the progression of diability in early parkinson's disease. *N Engl J Med*. 1993;328(3):176–183.
8. Gilgun-Sherki Y, Melamed E, Offen D. Oxidative stress induced-neurodegenerative diseases: the need for antioxidants that penetrate the blood brain barrier. *Neuropharmacology*. 2001;40(8):959–975.
9. Finkel T. Oxidant signals and oxidative stress. *Curr Opin Cell Biol*. 2003;15(2):247–254.
10. St-Pierre J, et al. Suppression of reactive oxygen species and neurodegeneration by the PGC-1 transcriptional coactivators. *Cell*. 2006;127(2):397–408.
11. Lee JM, Calkins MJ, Chan K, Kan YW, Johnson JA. Identification of the NF-E2-related factor-2-dependent genes conferring protection against oxidative stress in primary cortical astrocytes using oligonucleotide microarray analysis. *J Biol Chem*. 2003;278(14):12029–12038.
12. Wu Z, et al. Mechanisms controlling mitochondrial biogenesis and respiration through the thermogenic coactivator PGC-1. *Cell*. 1999;98(1):115–124.
13. Itoh K, et al. An Nrf2/small Maf heterodimer mediates the induction of phase II detoxifying enzyme genes through antioxidant response elements. *Biochem Biophys Res Commun*. 1997;236(2):313–322.
14. Itoh K, et al. Keap1 represses nuclear activation of antioxidant responsive elements by Nrf2 through binding to the amino-terminal Neh2 domain. *Genes Dev*. 1999;13(1):76–86.
15. Howden R. Nrf2 and cardiovascular defense. *Oxid Med Cell Longev*. 2013;2013:104308.
16. Joshi G, Johnson JA. The Nrf2-ARE pathway: a valuable therapeutic target for the treatment of neurodegenerative diseases. *Recent Pat CNS Drug Discov*. 2012;7(3):218–229.
17. Tan SM, de Haan JB. Combating oxidative stress in diabetic complications with Nrf2 activators: how much is too much? *Redox Rep*. 2014;19(3):107–117.
18. Mazzuferi M, Kumar G, van Eyll J, Danis B, Foerch P, Kaminski RM. Nrf2 defense pathway: Experimental evidence for its protective role in epilepsy. *Ann Neurol*. 2013;74(4):560–568.
19. Pomeshchik Y, et al. Does Nrf2 gene transfer facilitate recovery after contusion spinal cord injury? *Antioxid Redox Signal*. 2014;20(8):1313–1323.
20. Wang CY, et al. CD36 upregulation mediated by intranasal LV-NRF2 treatment mitigates hypoxia-induced progression of Alzheimer's-like pathogenesis. *Antioxid Redox Signal*. 2014;21(16):2208–2230.
21. Chen B, Tang L. Protective effects of catalase on retinal ischemia/reperfusion injury in rats. *Exp Eye Res*. 2011;93(5):599–606.
22. Rex TS, et al. Adenovirus-mediated delivery of catalase to retinal pigment epithelial cells protects neighboring photoreceptors from photo-oxidative stress. *Hum Gene Ther*. 2004;15(10):960–967.
23. Liu Y, Tang L, Chen B. Effects of antioxidant gene therapy on retinal neurons and oxidative stress in a model of retinal ischemia/reperfusion. *Free Radic Biol Med*. 2012;52(5):909–915.
24. Kanninen K, et al. Intrahippocampal injection of a lentiviral vector expressing Nrf2 improves spatial learning in a mouse model of Alzheimer's disease. *Proc Natl Acad Sci U S A*. 2009;106(38):16505–16510.
25. Nanou A, et al. Viral delivery of antioxidant genes as a therapeutic strategy in experimental models of amyotrophic lateral sclerosis. *Mol Ther*. 2013;21(8):1486–1496.
26. Fahim AT, Daiger SP, Weleber RG. Retinitis pigmentosa overview. In: Pagon RA, et al., eds. *GeneReviews*. Seattle, Washington, USA: University of Washington; 2000.
27. Ran X, et al. "RetinoGenetics": a comprehensive mutation database for genes related to inherited retinal degeneration. *Database (Oxford)*. 2014;2014:bau047.
28. Daiger SP, Sullivan LS, Bowne SJ. Genes and mutations causing retinitis pigmentosa. *Clin Genet*. 2013;84(2):132–141.
29. Shen J, et al. Oxidative damage is a potential cause of cone cell death in retinitis pigmentosa. *J Cell Physiol*. 2005;203(3):457–464.
30. Komeima K, Rogers BS, Lu L, Campochiaro PA. Antioxidants reduce cone cell death in a model of retinitis pigmentosa. *Proc Natl Acad Sci U S A*. 2006;103(30):11300–11305.
31. Usui S, et al. Increased expression of catalase and superoxide dismutase 2 reduces cone cell death in retinitis pigmentosa. *Mol Ther*. 2009;17(5):778–786.
32. Anderson D. The optic nerve in glaucoma. In: Tasman W, Jaeger EA, eds. *Duane's Ophthalmology*. Vol. 3. Philadelphia, Pennsylvania, USA: Lippincott Williams & Wilkins; 2013:Chapter 48.
33. Kanamori A, Catrinescu MM, Kanamori N, Mears KA, Beaubien R, Levin LA. Superoxide is an associated signal for apoptosis in axonal injury. *Brain*. 2010;133(9):2612–2625.
34. Lieven CJ, Hoegger MJ, Schlieve CR, Levin LA. Retinal ganglion cell axotomy induces an increase in intracellular superoxide anion. *Invest Ophthalmol Vis Sci*. 2006;47(4):1477–1485.
35. Taoka Y, Naruo M, Koyanagi E, Urakado M, Inoue M. Superoxide radicals play important roles in the pathogenesis of spinal cord injury. *Parapleigia*. 1995;33(8):450–453.
36. Kurimoto T, et al. Long-distance axon regeneration in the mature optic nerve: contributions of oncomodulin, cAMP, and pten gene deletion. *J Neurosci*. 2010;30(46):15654–15663.
37. de Lima S, et al. Full-length axon regeneration in the adult mouse optic nerve and partial recovery of simple visual behaviors. *Proc Natl Acad Sci U S A*. 2012;109(23):9149–9154.
38. Yin Y, et al. Oncomodulin is a macrophage-derived signal for axon regeneration in retinal ganglion cells. *Nat Neurosci*. 2006;9(6):843–852.
39. Park KK, et al. Promoting axon regeneration in the adult CNS by modulation of the PTEN/mTOR pathway. *Science*. 2008;322(5903):963–966.
40. Hoang QV, Linsenmeier RA, Chung CK, Curcio CA. Photoreceptor inner segments in monkey and human retina: mitochondrial density, optics, and regional variation. *Vis Neurosci*. 2002;19(4):395–407.
41. Nohl H, Hegner D. Do mitochondria produce oxygen radicals in vivo? *Eur J Biochem*. 1978;82(2):563–567.
42. Wellard J, Lee D, Valter K, Stone J. Photoreceptors in the rat retina are specifically vulnerable to both hypoxia and hyperoxia. *Vis Neurosci*. 2005;22(4):501–507.
43. Yu D, Cringle SJ, Su E, Yu PK. Intraretinal oxygen levels before and after photoreceptor loss in the RCS rat. *Invest Ophthalmol Vis Sci*. 2000;41(12):3999–4006.
44. Yu DY, Cringle SJ. Retinal degeneration and local oxygen metabolism. *Exp Eye Res*. 2005;80(6):745–751.
45. Watanabe S, Sanuki R, Ueno S, Koyasu T, Hasegawa T, Furukawa T. Tropisms of AAV for subretinal delivery to the neonatal mouse retina and its application for in vivo rescue of developmental photoreceptor disorders. *PLoS One*. 2013;8(1):e54146.
46. Natkunarajah M, et al. Assessment of ocular transduction using single-stranded and self-complementary recombinant adeno-associated virus serotype 2/8. *Gene Ther*. 2008;15(6):463–467.
47. Chang B, et al. Two mouse retinal degenerations caused by missense mutations in the beta-subunit of rod cGMP phosphodiesterase gene. *Vision Res*. 2007;47(5):624–633.
48. Punzo C, Kornacker K, Cepko CL. Stimulation of the insulin/mTOR pathway delays cone death in a mouse model of retinitis pigmentosa. *Nat Neurosci*. 2009;12(1):44–52.
49. Lee JM, Shih AY, Murphy TH, Johnson JA.

NF-E2-related factor-2 mediates neuroprotection against mitochondrial complex I inhibitors and increased concentrations of intracellular calcium in primary cortical neurons. *J Biol Chem*. 2003;278(39):37948–37956.
50. Gargini C, Terzibasi E, Mazzoni F, Strettoi E. Retinal organization in the retinal degeneration 10 (rd10) mutant mouse: a morphological and ERG study. *J Comp Neurol*. 2007;500(2):222–238.
51. Lem J, et al. Morphological, physiological, and biochemical changes in rhodopsin knockout mice. *Proc Natl Acad Sci U S A*. 1999;96(2):736–741.
52. Rohrer B, Lohr HR, Humphries P, Redmond TM, Seeliger MW, Crouch RK. Cone opsin mislocalization in Rpe65$^{-/-}$ mice: a defect that can be corrected by 11-cis retinal. *Invest Ophthalmol Vis Sci*. 2005;46(10):3876–3882.
53. Prusky GT, Alam NM, Beekman S, Douglas RM. Rapid quantification of adult and developing mouse spatial vision using a virtual optomotor system. *Invest Ophthalmol Vis Sci*. 2004;45(12):4611–4616.
54. De Lima S, Habboub G, Benowitz LI. Combinatorial therapy stimulates long-distance regeneration, target reinnervation, and partial recovery of vision after optic nerve injury in mice. *Int Rev Neurobiol*. 2012;106:153–172.
55. Moi P, Chan K, Asunis I, Cao A, Kan YW. Isolation of NF-E2-related factor 2 (Nrf2), a NF-E2-like basic leucine zipper transcriptional activator that binds to the tandem NF-E2/AP1 repeat of the f-globin locus control region. *Proc Natl Acad Sci U S A*. 1994;91(21):9926–9930.
56. Lee SY, et al. N-acetylcysteine promotes long-term survival of cones in a model of retinitis pigmentosa. *J Cell Physiol*. 2011;226(7):1843–1849.
57. Hauswirth WW, et al. Treatment of leber congenital amaurosis due to RPE65 mutations by ocular subretinal injection of adeno-associated virus gene vector: short-term results of a phase I trial. *Hum Gene Ther*. 2008;19(10):979–990.
58. Bainbridge JW, et al. Effect of gene therapy on visual function in Leber's congenital amaurosis. *N Engl J Med*. 2008;358(21):2231–2239.
59. Maguire AM, et al. Safety and efficacy of gene transfer for Leber's congenital amaurosis. *N Engl J Med*. 2008;358(21):2240–2248.
60. Clark J, Simon DK. Transcribe to survive: transcriptional control of antioxidant defense programs for neuroprotection in Parkinson's disease. *Antioxid Redox Signal*. 2009;11(3):509–528.
61. Malhotra D, et al. Global mapping of binding sites for Nrf2 identifies novel targets in cell survival response through ChIP-Seq profiling and network analysis. *Nucleic Acids Res*. 2010;38(17):5718–5734.
62. Thimmulappa RK, Mai KH, Srisuma S, Kensler TW, Yamamoto M, Biswal S. Identification of Nrf2-regulated genes induced by the chemopreventive agent sulforaphane by oligonucleotide microarray. *Cancer Res*. 2002;62(18):5196–5203.
63. Reisman SA, Yeager RL, Yamamoto M, Klaassen CD. Increased Nrf2 activation in livers from Keap1-knockdown mice increases expression of cytoprotective genes that detoxify electrophiles more than those that detoxify reactive oxygen species. *Toxicol Sci*. 2009;108(1):35–47.
64. Fox RJ, et al. Placebo-controlled phase 3 study of oral BG-12 or glatiramer in multiple sclerosis. *N Engl J Med*. 2012;367(12):1087–1097.
65. Gold R, et al. Placebo-controlled phase 3 study of oral BG-12 for relapsing multiple sclerosis. *N Engl J Med*. 2012;367(12):1098–1107.
66. Saint-Geniez M, et al. PGC-1α regulates normal and pathological angiogenesis in the retina. *Am J Pathol*. 2013;182(1):255–265.
67. Ciron C, Lengacher S, Dusonchet J, Aebischer P, Schneider BL. Sustained expression of PGC-1α in the rat nigrostriatal system selectively impairs dopaminergic function. *Hum Mol Genet*. 2012;21(8):1861–1876.
68. Izzott A, Bagnis A, Sacca S. The role of oxidative stress in glaucoma. *Mutat Res*. 2006; 612(2):105–114.
69. Beatty S, Koh H, Henson D, Boulton M. The role of oxidative stress in the pathogenesis of age-related macular degeneration. *Surv Ophthalmol*. 2000;45(2):115–134.
70. Justilien V, et al. SOD2 knockdown mouse model of early AMD. *Invest Ophthalmol Vis Sci*. 2007;48(10):4407–4420.
71. Girmens JF, Sahel JA, Marazova K. Dry age-related macular degeneration: a currently unmet clinical need. *Intractable Rare Dis Res*. 2012;1(3):103–114.
72. Streichert LC, Birnbach CD, Reh TA. A diffusible factor from normal retinal cells promotes rod photoreceptor survival in an in vitro model of retinitis pigmentosa. *J Neurobiol*. 1999;39(4):475–490.
73. Mohand-Said S, Hicks D, Dreyfus H, Sahel JA. Selective transplantation of rods delays cone loss in a retinitis pigmentosa model. *Arch Ophthalmol*. 2000;118(6):807–811.
74. Léveillard T, et al. Identification and characterization of rod-derived cone viability factor. *Nat Genet*. 2004;36(7):755–759.
75. Steinberg RH. Survival factors in retinal degenerations. *Curr Opin Neurobiol*. 1994;4(4):515–524.
76. Mohand-Saïd S, et al. Normal retina releases a diffusible factor stimulating cone survival in the retinal degeneration mouse. *Proc Natl Acad Sci U S A*. 1998;95(14):8357–8362.
77. Gupta N, Brown KE, Milam AH. Activated microglia in human retinitis pigmentosa, late-onset retinal degeneration, and age-related macular degeneration. *Exp Eye Res*. 2003;76(4):463–471.
78. Cepko CL. Emerging gene therapies for retinal degenerations. *J Neurosci*. 2012;32(19):6415–6420.
79. Busskamp V, et al. Genetic reactivation of cone photoreceptors restores visual responses in retinitis pigmentosa. *Science*. 2010;329(5990):413–417.
80. Himori N, et al. Critical role of Nrf2 in oxidative stress-induced retinal ganglion cell death. *J Neurochem*. 2013;127(5):669–680.
81. Yoritaka A, Hattori N, Uchida K, Tanaka M, Stadtman ER, Mizuno Y. Immunohistochemical detection of 4-hydroxynonenal protein adducts in Parkinson disease. *Proc Natl Acad Sci U S A*. 1996;93(7):2696–2701.
82. Castellani R, Smith MA, Richey PL, Perry G. Glycoxidation and oxidative stress in Parkinson disease and diffuse Lewy body disease. *Brain Res*. 1996;737(1):195–200.
83. Floor E, Wetzel MG. Increased protein oxidation in human substantia nigra pars compacta in comparison with basal ganglia and prefrontal cortex measured with an improved dinitrophenylhydrazine assay. *J Neurochem*. 1998;70(1):268–275.
84. Schapira AH, Cooper JM, Dexter D, Jenner P, Clark JB, Marsden CD. Mitochondrial complex I deficiency in Parkinson's disease. *Lancet*. 1989;1(8649):1269.
85. Chomyn A, Attardi G. MtDNA mutations in aging and apoptosis. *Biochem Biophys Res Commun*. 2003;304(3):519–529.
86. Bender A, et al. High levels of mitochondrial DNA deletions in substantia nigra neurons in aging and Parkinson disease. *Nat Genet*. 2006;38(5):515–517.
87. Matigian N, et al. Disease-specific, neurosphere-derived cells as models for brain disorders. *Dis Model Mech*. 2010;3(11–12):785–798.
88. Ramsey CP, et al. Expression of Nrf2 in neurodegenerative diseases. *J Neuropathol Exp Neurol*. 2007;66(1):75–85.
89. Kaidery NA, et al. Targeting Nrf2-mediated gene transcription by extremely potent synthetic triterpenoids attenuate dopaminergic neurotoxicity in the MPTP mouse model of Parkinson's disease. *Antioxid Redox Signal*. 2013;18(2):139–157.
90. Gan L, Vargas MR, Johnson DA, Johnson JA. Astrocyte-specific overexpression of Nrf2 delays motor pathology and synuclein aggregation throughout the CNS in the alpha-synuclein mutant (A53T) mouse model. *J Neurosci*. 2012;32(49):17775–17787.
91. Solis LM, et al. Nrf2 and Keap1 abnormalities in non-small cell lung carcinoma and association with clinicopathologic features. *Clin Cancer Res*. 2010;16(14):3743–3753.
92. Zhang P, et al. Loss of Kelch-like ECH-associated protein 1 function in prostate cancer cells causes chemoresistance and radioresistance and promotes tumor growth. *Mol Cancer Ther*. 2010;9(2):336–346.
93. Ryan D, King A, Thomas G. Cleavage of foot-and-mouth disease virus polyprotein is mediated by residues located within a 19 amino acid sequence. *J Gen Virol*. 1991;72(11):2727–2732.
94. Grieger JC, Choi VW, Samulski RJ. Production and characterization of adeno-associated viral vectors. *Nat Protoc*. 2006;1(3):1412–1428.
95. Vandenberghe LH, Xiao R, Lock M, Lin J, Korn M, Wilson JM. Efficient serotype-dependent release of functional vector into the culture medium during adeno-associated virus manufacturing. *Hum Gene Ther*. 2010;21(10):1251–1257.
96. Matsuda T, Cepko CL. Electroporation and RNA interference in the rodent retina in vivo and in vitro. *Proc Natl Acad Sci U S A*. 2004;101(1):16–22.
97. Wang S, Sengel C, Emerson M, Cepko C. The binary decision of rod and bipolar fate in the vertebrate retina is controlled by a gene regulatory network. *Dev Cell*. 2014;30(5):513–527.
98. Douglas RM, Alam NM, Silver BD, McGill TJ, Tschetter WW, Prusky GT. Independent visual threshold measurements in the two eyes of freely moving rats and mice using a virtual-reality optokinetic system. *Vis Neurosci*. 2005;22(5):677–684.